Article

Numerical Simulations of the Hydraulic Performance of a Breakwater-Integrated Overtopping Wave Energy Converter

Giuseppina Palma [1], Sara Mizar Formentin [1], Barbara Zanuttigh [1], Pasquale Contestabile [2,3] and Diego Vicinanza [2,3,4,*]

[1] Department of Civil, Chemical, Environmental and Materials Engineering, University of Bologna, Viale Eisorgimento 2, 40136 Bologna, Italy; giuseppina.palma2@unibo.it (G.P.); saramizar.formentin2@unibo.it (S.M.F.); barbara.zanuttigh@unibo.it (B.Z.)

[2] Department of Engineering, University of Campania, via Roma 29, 81031 Aversa, Caserta, Italy; pasquale.contestabile@unicampania.it

[3] Inter-University National Consortium for Marine Sciences (CoNISMa), 00196 Roma, Italy

[4] Stazione Zoologica Anton Dohrn, Villa Comunale, 80121 Napoli, Italy

[*] Correspondence: diego.vicinanza@unicampania.it; Tel.: +39-081-5010245

check for updates

Abstract: OBREC is the acronym that stands for Overtopping Breakwater for Energy Conversion. It is a multifunctional device aimed to produce energy from the waves, while keeping the harbour area protected from flooding. In this paper, the inclusions of a berm to reduce wave reflection, the shape of the sloping plate to maximise wave overtopping and the reservoir width and the crown wall shape to maximise wave energy capture while keeping the harbour safety were analysed to optimize the hydraulic and structural performances of the device. Several configurations were numerically investigated by means of a 2DV RANS-VOF code to extend the results already obtained during previous experimental campaigns. The wave reflection coefficient, the average wave overtopping flows and the wave loadings along the structure are computed, compared with existing formulae and discussed with reference to the OBREC prototype installed in the Port of Naples.

1. Introduction

The development of installations aimed to exploit marine energy has been subjected to an increasing interest in the recent years, since it represents a way to face the growing energy demand, limit the emissions and promote adaptations to climate change [1–6]. Furthermore, farms composed of wave energy converters are shown to be effective against erosion and flooding, supporting the protection of the coastal area as demonstrated by Rodrigo-Delgado and Bergillos' studies [7–10].
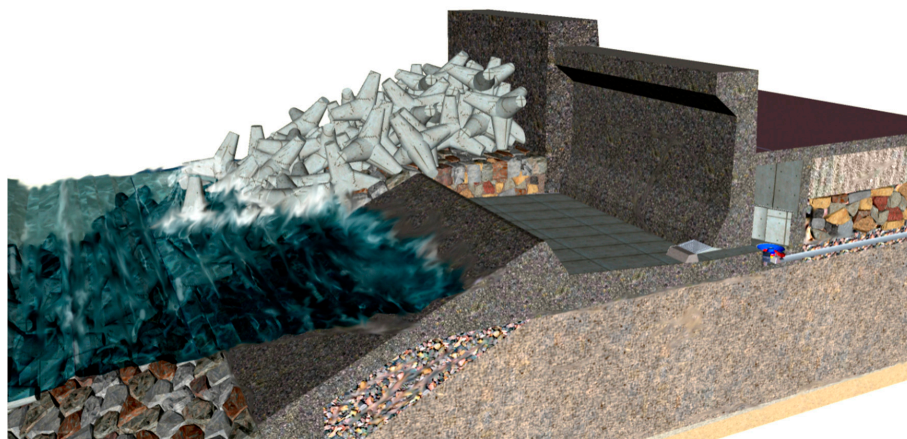
The ocean can provide a vast amount of energy [11]. Indeed, the wave energy power is enormous and more reliable than other renewable resources, such as solar and wind energy, due to its density (2–3 kW/m^2) that is greater (wind: 0.4–0.6 kW/m^2; solar: 0.1–0.2 kW/m^2) [12]. However, the marine technologies, the Wave Energy Converters (WECs) among others, are still at immature stages to be commercialized successfully in the market [13,14]. Despite this, more than 1000 WECs have been developed worldwide and more than 140 are patented [15].

The main obstacle which limits the growth of this energy sector is strictly related to the design reliability and economic feasibility of these installations. To overcome technological barriers and minimize conflict of uses, the European Commision initiative "Oceans of Tomorrow" aimed at the development of multipurpose offshore areas, leading to the three FP7 funded projects: TROPOS [16],

MERMAID [17] and H2OCEAN [18]. These projects analyzed the possibility to combine marine renewable energy with aquaculture, maritime transport and leisure activities. The purposes of such multifunctional solutions [19,20] are to (i) promote the use of resource diversity (wind, wave and tide), so that the variability of the available power can be reduced [21]; (ii) develop technical synergies, minimising environmental impacts and obtaining economic benefits [22]; and (iii) lower the system integration costs and facilitate the licensing issues [23].

Offshore installations maximize the energy harvesting, but their distance from the shore affects the amount and the costs of energy transfers. Therefore, attractive solutions may be on-shore WECs integrated in coastal or harbor structures. The research on this topic focused on the development of Oscillating Water Column devices (OWC), a.o. the REWEC3 [24] installed in the Civitavecchia harbor (Italy), the PICO [25], the LIMPET [26] and the MUTRIKU [27] power plants. The need to use a different principle of exploitation and several issues related to some of these installations, such as the acoustic pollution for the MUTRIKU case [28], brought the attention to the overtopping devices as the Sea-wave Slot-cone Generator [29], which however was economically unfeasible due to the complex geometry of the reservoir.

In this context, an innovative solution was developed by the University of Campania "Luigi Vanvitelli": The Overtopping Breakwater for the Energy Conversion, OBREC hereinafter [30] (Figure 1). It is a rubble mound breakwater for harbor protection including a top-front reservoir that captures the overtopped water to produce electricity by using the difference in water levels between the reservoir and the mean sea water level. The energy is then extracted via low head turbines, installed inside the wave chamber located at the rear side of the crown wall.

Figure 1. A 3-D rendering of a traditional rubble-mound breakwater and the Overtopping Breakwater for the Energy Conversion (OBREC).

The OBREC has been studied already during some experimental campaigns [30–32] and has been recently installed in the Port of Naples in September 2015 [33]. The 2 laboratory campaigns were aimed (i) to analyse the device by comparing it with a traditional rubble mound breakwater and (ii) to evaluate its hydraulic and structural performance under ordinary and extreme conditions.

The purpose of this paper is to extend the experimental database, providing a greater understanding of the structure response by analyzing the effects of some fundamental geometrical parameters on the OBREC performance in terms of energy production, structural stability and harbor safety. This assessment has been carried out by means of 2DV numerical modelling, i.e., IH2-VOF. The results of the experimental campaigns have been used to calibrate the model. The original laboratory OBREC cross section has been then modified to perform a sensitivity analysis under ordinary and extreme conditions.

The paper structure is as follows. Section 2 describes the experimental and numerical set-up, including the wave flume characteristics, the data collection and the results of the calibration. Section 3 presents the sensitivity analysis performed by varying some geometrical parameters of the OBREC
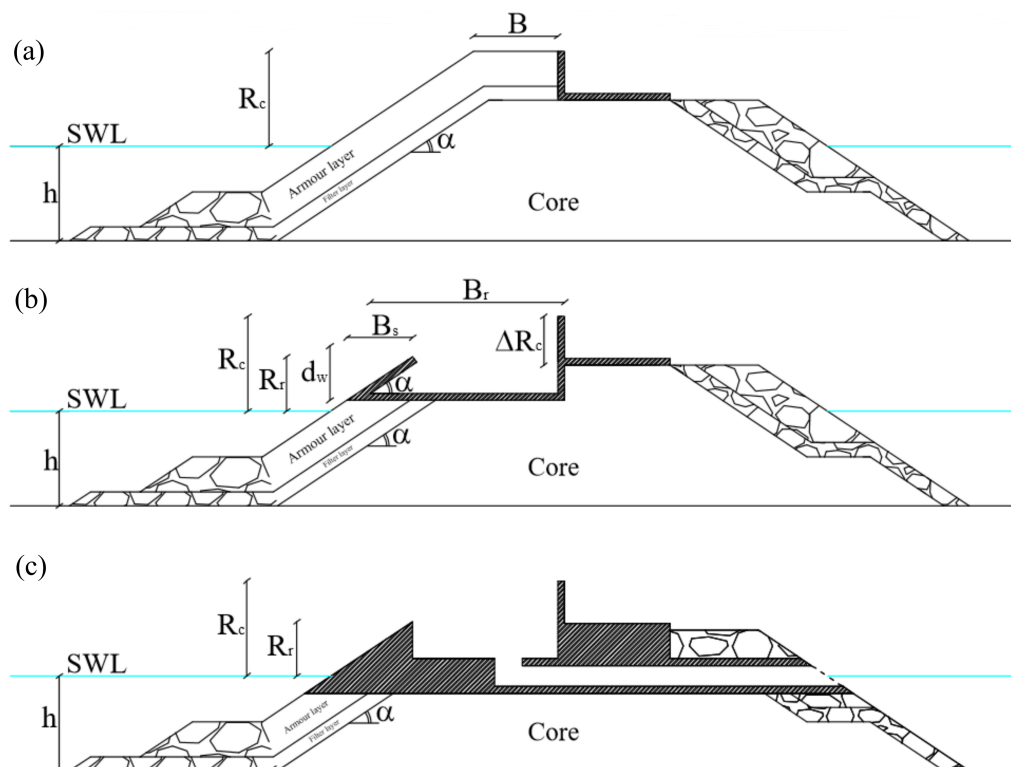
cross section. This analysis is divided into 3 main parts addressing (1) the OBREC hydraulic performance by analyzing the reflection coefficient K_r and the average overtopping flow inside the reservoir $q_{reservoir}$; (2) the structural performance in terms of pressures acting on the device; and (3) the harbor safety by measuring the average overtopping flow at the rear side of the rear wall q_{rear}. Section 4 discusses the results obtained with reference to the OBREC pilot plant installed in the port of Naples in 2017. Some conclusions and recommendations on the OBREC design optimizations are drawn in Section 5.

2. Material and Methods

This section presents the set-up of the numerical model based on the experiments performed by Vicinanza [30] at Aalborg University in Denmark. The numerical simulations have been carried out by means of the IH-2VOF single phase code, a 2DV Rans-VOF code developed by the University of Cantabria [34] and already widely adopted for design purposes of the coastal and harbor structures. The OBREC cross section (Section 2.1), the wave flume and the mesh characteristics (Section 2.2), the tested wave conditions and the position of the gauges (Section 2.3), and the results of the model calibration (Section 2.4) are presented and discussed.

2.1. The Overtopping Breakwater for the Energy Conversion Cross Section

The idea behind the OBREC device implies the modification of a traditional rubble mound breakwater (Figure 2a), where the crest and the upright section are replaced by a concrete reservoir. Figure 2b shows the main OBREC geometric parameters, where B_r is the reservoir width, B_s the horizontal extension of the sloping plate, α its inclination (equals to 34° in the physical model), d_w is the height of the sloping plate and R_r and R_c are the freeboard crests (with respect to the mean sea water level) of the sloping plate and of the rear wall, respectively.

Figure 2. (**a**) The traditional rubble mound breakwater, (**b**) the OBREC physical model, and (**c**) the OBREC numerical model (adapted from Vicinanza 2014 [26], with permission from ELSEVIER, 2018). The main geometric parameters are: B_r the reservoir width, B_s the horizontal extension of the sloping plate, α its inclination, d_w the height of the sloping plate and R_r and R_c the freeboard crests of the sloping plate and of the rear wall, respectively.

The 2012 campaign involved the testing of two configurations of the OBREC cross section, characterized by a different height of the sloping plate: $d_{w,low}$ = 2.25 m and $d_{w,high}$ = 3.75 m at prototype scale. In this paper, the numerical model is calibrated considering only the $d_{w,high}$ configuration.

To guarantee the numerical stability of the simulations and the correct representation of the physical processes, the cross section in the numerical model was slightly modified as follows.

During the experiments, the water was pumped out from the reservoir by means of external pipes, which were insufficient to avoid the saturation of the reservoir during the extreme tests (see Section 2.3). The numerical cross section was modified by including an internal pipe from the reservoir bottom to the structure inshore slope to allow the water to freely flow into the reservoir and the testing of the potential energy production during operating conditions.

The thickness of the OBREC slab foundation was slightly increased (see Figure 2c) to avoid numerical instabilities induced by the limited thickness of the impermeable layer over the permeable structure in the run-up/down area, i.e., in an area characterized by very frequent changes of wet/dry conditions.

The differences between the experimental and the numerical cross sections affect the reflection phenomenon because in the latter case, the thickness of the impermeable part has been increased. However, this does not affect the overtopping phenomenon as shown by the results of the calibration, i.e., Section 2.4.

The breakwater used during the experiments, in which OBREC has been introduced, is composed of a rock armour, a filter layer and a core. The average size of the rocks are D_{n50} = 40 mm for the armour layer, D_{n50} = 20 mm for the filter layer and D_{n50} = 2 mm for the core. In the numerical model, the aforementioned porous layers are characterized by several parameters as the porosity itself n, the added mass coefficient c_A, the linear α and non-linear β friction coefficients. These last two parameters describe respectively the laminar and the turbulent flow properties in between the stones by means of the Forchheimer equation [35], defined as

$$\frac{dh}{dx} = i = au_f + bu_f^2 + c\frac{\partial u}{\partial t} \tag{1}$$

where

$$a = \alpha \frac{(1-n)^2}{n^3} \cdot \frac{\nu}{gD_{n,50}^2} \tag{2}$$

$$b = \beta \frac{1-n}{n^3} \cdot \frac{\nu}{gD_{n,50}} \tag{3}$$

In Equations (1)–(3), u_f is the porous flow velocity averaged over the total sample area (grains), g the gravitational acceleration and ν the fluid kinematic viscosity. In Equation (1), the third term on the right-hand side is usually small and therefore neglected. The β coefficient has been set equal to 1000, while α was set to 1.1, 1.0 and 0.8 for the armour, the filter and the core layers, respectively. These values have been defined based on the literature [36–38].

The model calibration has been performed by varying the porosity values and by keeping constant all the other parameters (see Section 2.4) to optimize the representation of the hydraulic performance of the device.

2.2. Wave Conditions and Measurements

The 2012 experimental campaign involved 48 tests under normal and extreme conditions. The irregular wave series have been generated based on the three JONSWAP spectrum parameters: the wave height H_{m0}, the peak frequency f_p and the so-called peak enhancement factor γ (3.3 in all the tests). The wave series considered at least 1000 waves.

The numerical simulations have been carried out by defining H_{m0}, γ, the spectral wave period $T_{m-1,0}$, the water depth in the generation area h and the duration of the simulation t. The simulation

program was divided into two test series, "normal" (representing poor and mild wave climate) and "extreme" (representative of a severe storm condition). Table 1 contains the characteristics of both the normal and extreme wave conditions. Each numerical test considers at least 500 waves, which are sufficient to perform a statistical wave overtopping analysis as demonstrated by Romano [39].

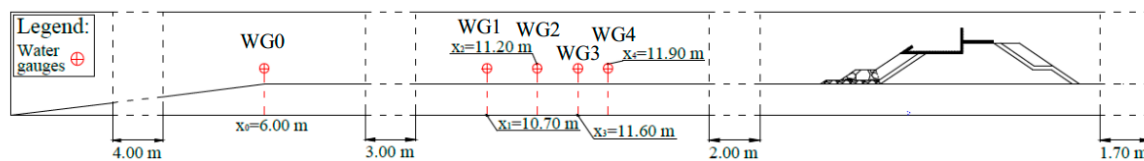**Table 1.** The characteristics of the ordinary and extreme wave conditions.

Tests	h (m)	H_{m0} (m)	$T_{m-1,0}$ (s)	R_c (m)	R_r (m)
Normal	0.27	0.077–0.149	1.327–2.090	0.155	0.27
Extreme	0.34	0.193	2.233	0.085	0.20

All the normal wave conditions—except for the one characterized by the smallest wave height H_{m0} (0.077 m)—are characterized by the same H_{m0} but different spectral wave periods $T_{m-1,0}$. Therefore, the tests chosen allowed the analysis of the hydraulic performance according to the wave steepness s_o.

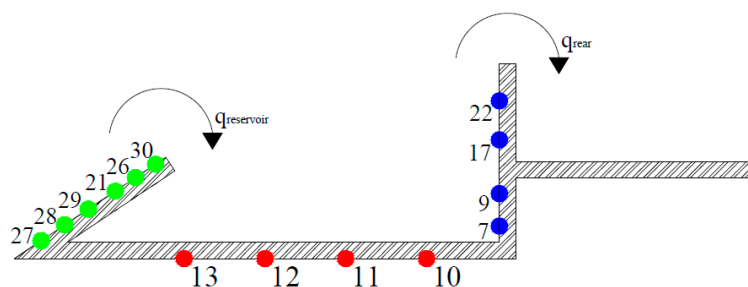Several wave gauges (WGs) have been installed inside the numerical channel to evaluate

- the reflection coefficient K_r, in normal conditions;
- the average overtopping discharge inside the reservoir $q_{reservoir}$, in normal conditions;
- the pressures p acting on the structure, under extreme conditions;
- the average overtopping discharge at the rear side of the crown wall q_{rear}, under extreme conditions.

A 3-point method [40] has been applied to derive the reflection coefficient K_r, by using WG1, WG2 and WG3 in Figure 3, located in front of the structure. The offshore wave gauge, WG0, has been used to measure the generated wave height.

Figure 3. The positions of the wave gauges for the evaluation of K_r.

The numerical pressure transducers have been placed along the structure in the same position as in the laboratory experiments (Figure 4). The sensors 13, 12, 11 and 10, during the experiments, have been used to evaluate the uplift pressures, while in the numerical simulations, also the downward ones.

Figure 4. The positions of the water gauges to evaluate (1) the pressure acting on the device and (2) the $q_{reservoir}$ and q_{rear}.

The average overtopping discharges at the rear side of the OBREC (q_{rear}) was determined in the lab by using a ramp to guide the overtopping wave volumes into a box. A depth gauge was installed in the box to measure the overtopping discharge and to control the pump to empty the box at a given threshold level. Similarly, the overtopping discharge in the front reservoir ($q_{reservoir}$) was measured using depth gauges, which controlled several pumps. The 2-D model has been provided with a pipe to

let the overtopping water flows towards the inshore edge, and two WGs were placed on the top of the sloping plate and at the rear side of the rear wall to estimate respectively the values of $q_{reservoir}$ and q_{rear} (Figure 4). The overtopping discharges have been derived by integrating (along the vertical) cell by cell the horizontal velocity component multiplied by the cell height (i.e., z direction).

2.3. Numerical Wave Flume and Mesh

The wave flume has been reproduced in the numerical model at the model scale. The flume is 20 m long with a 1:20 slope for the first 6 m that is followed by a horizontal bottom. Such a foreshore has been introduced to guarantee the wave generation in intermediate water depths.

The mesh for the numerical domain has been divided into three zones along the flume (in the x direction) and one along the vertical (in the z direction). The extension and the resolution of these zones depend on the position of the structure. The characteristics of the computational grid have been defined to ensure a good compromise between the accuracy of the results and the computational cost. The first zone corresponds to the wave generation and transformation along the foreshore, while the third one is inshore the structure. They are 16.05 and 2.51 m long, respectively, and both of them have been provided with a grading mesh more refined close to the structure, with a minimum cell size of 1 cm. The central zone, 1.44 m long, consider the run-up/down area over the structure, where the run-up/down and the overtopping occurs. Therefore, it has been provided with a regular grid, according to the tested wave characteristics, with a minimum cell size of 1×1 cm, avoiding discontinuities along the computational grid.

2.4. Calibration of the 2-D Numerical Model

Following Palma [41], the calibration of the 2-D numerical model has been performed considering, at the same time, the representation of K_r and $q_{reservoir}$ under normal conditions. This procedure implied the variation of the porosity n assigned to the layers of the breakwater, under the same wave attack. Table 2 reports the values assigned to each layer together with the comparison between the experimental $q_{res,exp}$ and the numerical $q_{res,num}$ discharge flows. The final n has been defined according to the best agreement, i.e., configuration 2 in Table 2.

Table 2. The experimental vs. numerical $q_{reservoir}$ obtained by varying the porosities n assigned to the layers of the breakwater, i.e., armour, filter and core.

Configuration	Armour	Filter	Core	$q_{res,exp}$ (L/m/s)	$q_{res,num}$ (L/m/s)
1	0.8	0.7	0.6	0.046	0.073
2	0.7	0.6	0.5	0.046	0.056
3	0.6	0.5	0.4	0.046	0.006
4	0.7	0.5	0.4	0.046	0.004

The 2-D numerical model has been tested then under all the normal wave conditions, already presented in Table 1, to determine K_r, $q_{reservoir}$ and therefore the reliability of the numerical model. In order to compare the numerical $q_{reservoir}$ with the experimental values and the theoretical formulations, they have been non-dimensionalised. Furthermore, by following the definition proposed by Ahrens and Heimbaugh (1986, Equation (4)) [42], it has been possible to take into account the difference between the wave spectra generated in the lab and in the numerical wave channel, thanks to the presence of the significant wave height H_{m0} in Equation (4). The theoretical formulae considered to evaluate the overtopping discharge are reported in Equations (5) and (6) and correspond to those adopted in the EurOtop 2016 [43] to assess the same phenomenon on the slopes such as dikes, levees and embankments.

$$q^*_{reservoir} = \frac{q}{\sqrt{g \cdot H_{m0}{}^3}} \tag{4}$$

with a maximum of

$$\frac{q}{\sqrt{g \cdot H_{m0}^3}} = \frac{0.023}{\sqrt{tan\ \alpha_{off}}} \cdot \gamma_b \cdot \xi_{m-1,0} \cdot exp\left[-\left(2.7\frac{R_r}{\xi_{m-1,0} \cdot H_{m0} \cdot \gamma_b \cdot \gamma_f \cdot \gamma_\beta \cdot \gamma_v}\right)^{1.3}\right] \tag{5}$$

$$\frac{q}{\sqrt{g \cdot H_{m0}^3}} = 0.09 \cdot exp\left[-\left(1.5\frac{R_r}{H_{m0} \cdot \gamma_f \cdot \gamma_\beta}\right)^{1.3}\right] \tag{6}$$

In Equations (5) and (6), α_{off} is the offshore slope angle, while γ_b is the berm influence factor, γ_f is the roughness influence factor, γ_β is the oblique wave action influence factor, γ_v is the influence factor for a vertical wall, $\xi_{m-1,0}$ is the breaker parameter and R_r is the freeboard crest of the sloping plate.

Figure 5 shows that the numerical model slightly and systematically overestimates the reflection coefficients. The deviation is on average equal to 15%, and it increases with the increasing of s_o. The reason can be addressed to the slight modification occurred in modelling the cross section for the numerical analysis, concerning the thickness of the impermeable part as described in Section 2.1. (Figure 2b,c). However, such modification has no implication in the representation of the discharge flows inside the reservoir, i.e., $q_{reservoir}$. In fact, Figure 6 shows that the numerical $q^*_{reservoir}$ gives a better estimation of the laboratory results. This is confirmed by the performed statistical analysis. Indeed, the difference among the experimental, the numerical and the theoretical values obtained are statistically computed by means of 2 parameters, describing the error made, i.e., the root mean square error (RMSE) and the Willmott index (WI) [44], defined in Equations (7) and (8), respectively. The quantity "y" represents the dimensionless discharge rate, defined in Equation (4). The subscripts "s" stands for the experimental data, while "mod" for the numerical and the theoretical ones are according to the analysis performed. Therefore, "$\overline{y}_s$" is the mean of the experimental discharge flows. A good representation of the experimental data is characterized by a RMSE value close to 0 and WI values close to 1. Indeed, the numerical RMSE and WI are equal to 0.005 and 0.75, while the theoretical ones to 0.007 and 0.59, respectively.
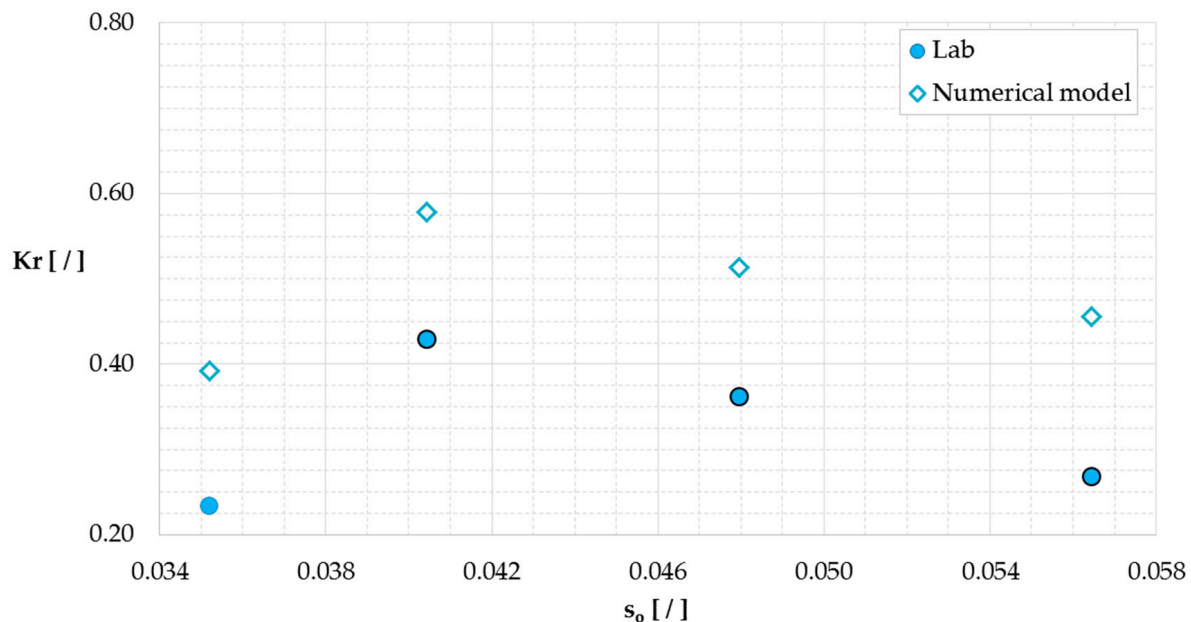

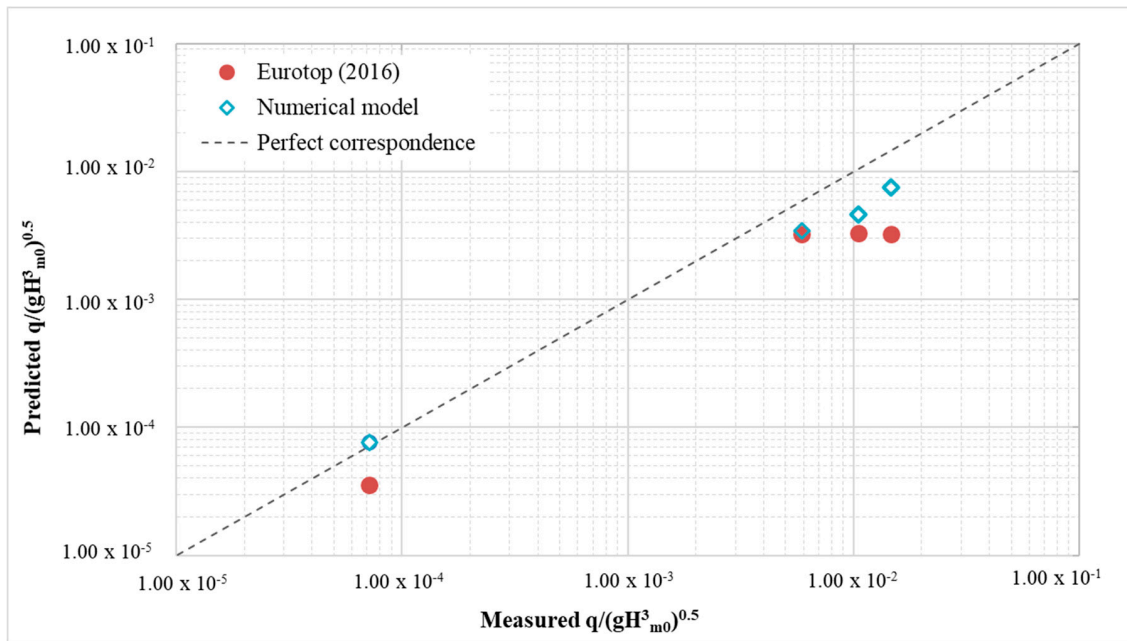**Figure 5.** The laboratory vs. numerical model *Kr* for the normal wave conditions only.

Figure 6. The numerical and theoretical vs. laboratory $q^*_{reservoir}$ for the normal wave conditions.

$$RMSE = \sqrt{\frac{1}{N} \sum_{j=1}^{N} \left(y_{s,j} - y_{mod,j}\right)^2} \tag{7}$$

$$WI = 1 - \frac{\sum_{j=1}^{N} \left(y_{s,j} - y_{mod,j}\right)^2}{\sum_{j=1}^{N} \left[|y_{s,j} - \overline{y}_s| + |y_{mod,j} - \overline{y}_s|\right]^2} \tag{8}$$
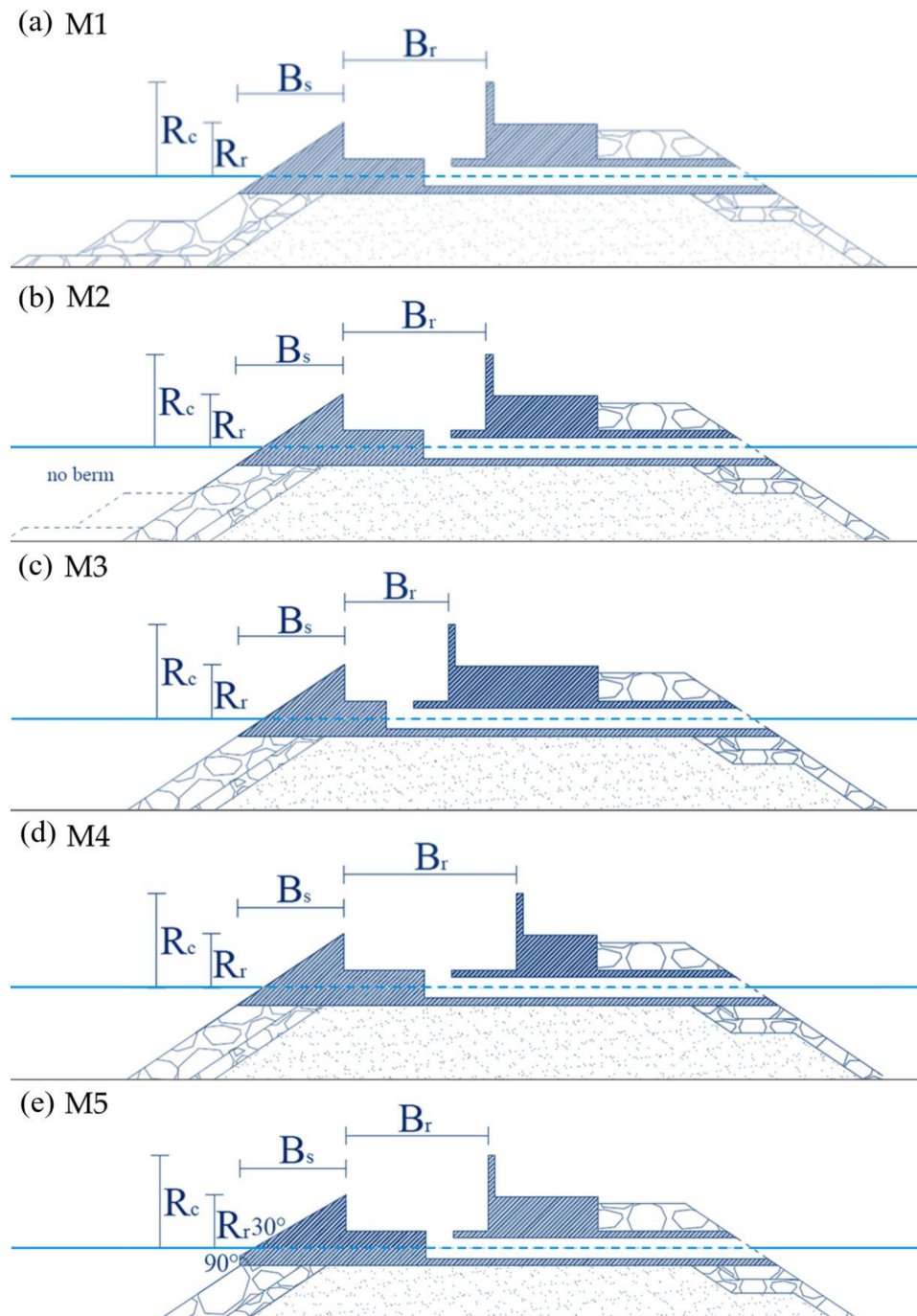
The difference between the experiments and the formulae was expected, as the formulae are essentially based on traditional structures and the calibration of the roughness factor is insufficient to allow greater accuracy [30].

2.5. Tested Configurations

A sensitivity analysis has been carried out by using five different geometries which differ from the original one by changing one geometric parameter at once. The aim is to propose a design for the OBREC that maximizes the device exploitability, while obtaining the best compromise among energy production, harbor safety and easy installation. Specifically, the selected parameters were the reservoir width B_r and the shape of the sloping plate (its inclination a), while the sloping plate freeboard R_r and its longitudinal dimension of B_s have been kept constant. Figure 7 shows all the tested configurations (named M1–M5), which the main parameters of are synthesized in Table 3.

M1 reproduces the 2012 laboratory configuration, as shown in Figure 2c. The differences between the laboratory and the numerical models have been already discussed in the previous section. This configuration represents a benchmark case in which it is possible to analyze the relevance of the berm in the wave-structure interactions. As a matter of fact, M2 corresponds to M1 except for the presence of this element (see Figure 7a,b).

To analyze properly all the parameters related to the OBREC device, M2 has been chosen as the reference configuration. The compatibility of this kind of installations in breakwaters, not provided with a berm, has been already analyzed during the second laboratory campaign, Iuppa [31]. Therefore, the other selected OBREC cross sections differ from M2 only for a geometric parameter at once, allowing the assessment of the effects of a specific element on the hydraulic and structural performances.

Figure 7. (**a**) The original $d_{w,high}$ configuration (M1); (**b**) the configuration without a berm (M2); (**c**) B_r = 0.3 m (M3); (**d**) B_r = 0.5 m (M4); and (**e**) the sloping plate $90° + 30°$ (M5).

Table 3. The geometrical characteristics of the configurations analyzed (Figure 7).

Configuration	Berm	R_c (m)	R_r (m)	B_s (m)	B_r (m)	$\alpha_{off, plate}$ (°)
M1	√	0.27	0.155	0.3074	0.41	34°
M2	×	0.27	0.155	0.3074	0.41	34°
M3	×	0.27	0.155	0.3074	0.30	34°
M4	×	0.27	0.155	0.3074	0.50	34°
M5	×	0.27	0.155	0.3074	0.41	$90° + 30°$

The configurations M3 and M4 have been selected to analyse the change in the reservoir width B_r. The two cross sections imply a variation of B_r of 25% with respect to the benchmark case. The aim of this analysis is to assess its relevance in the saturation of the reservoir, the maximization of the energy production, the limitation of the pressures along the crown wall and the values of q_{rear}.

The configuration M5 (Figure 7e) differs in the shape of the sloping plate. This section has been designed according to the results obtained from the research aimed to optimize the WECs profile. Kofoed [45] proved that the adoption of a 30° inclined slope angle improves the hydraulic performance in terms of overtopping discharge. This result has been then validated by Nam [46]. Such authors considered also a double inclination for the ramp shape, with the submerged part having a vertical orientation, demonstrating its positive effects in increasing the run-up.
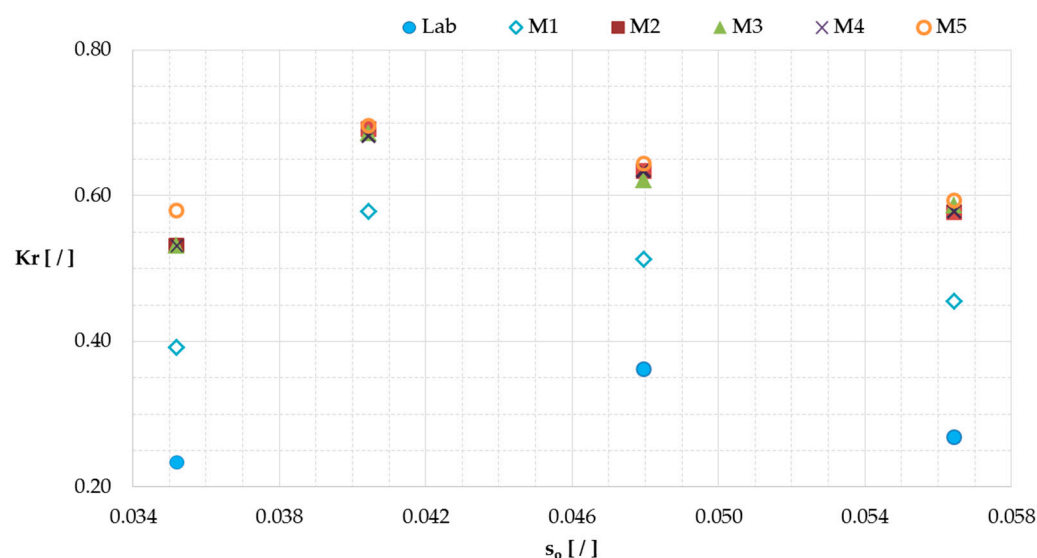
3. Results

This section shows the results from numerical simulations using the calibrated IH2VOF model. Section 3.1 focuses on the description of the hydraulic performance in normal conditions. Instead, the effect of geometric changes and on the loads and harbor safety in extreme conditions are reported in Sections 3.2 and 3.3, respectively. The results obtained in terms of K_r, $q_{reservoir}$, q_{rear} and pressures are used to improve the design of the device, by providing some general guidelines according to the analysis of the wave–structure interactions.

3.1. Effects of Geometric Changes on the Hydraulic Performance

The hydraulic performance of the OBREC device are here analyzed in terms of K_r and non-dimensional overtopping at the rear of the structure, $q*_{reservoir}$, under normal conditions.

Figure 8 shows the values of K_r versus the steepness s_o for all the configurations, under normal conditions. The laboratory results (already shown in Figure 5) is respected. The configuration M2 leads to greater values with respect to M1. This result was expected considering the work of Zanuttigh [47], who demonstrated that structures characterized by a submerged berm lead to a smaller K_r than those with a straight slope validated also by the study performed by Formentin [48]. The design of a toe protection in case of an OBREC installation in a breakwater without berm should be taken into account.
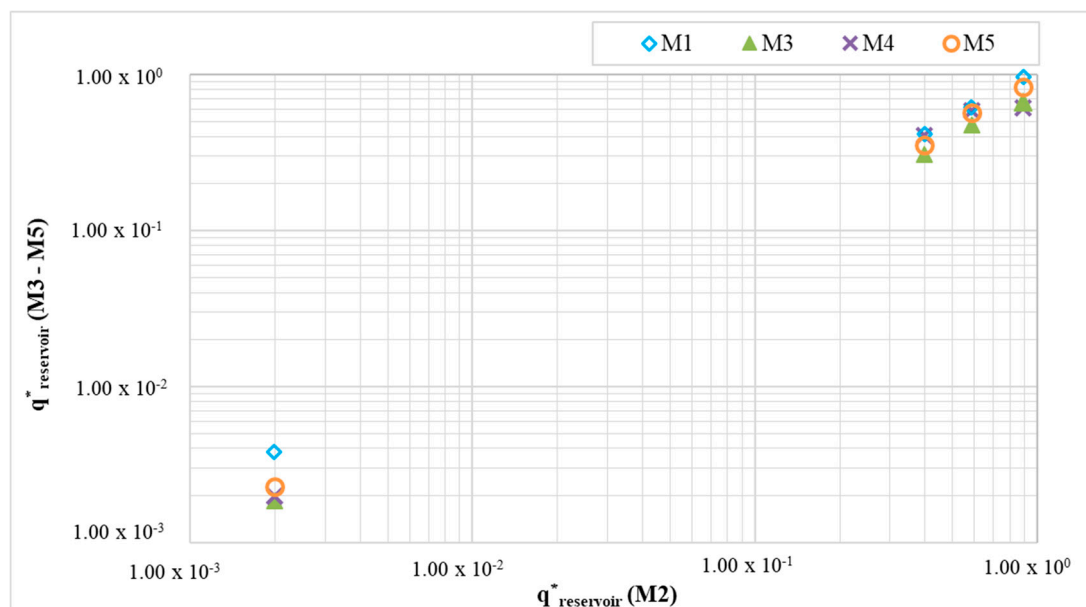

Figure 8. A comparison of the values of K_r for the M1–M5 configurations, under normal conditions only (Table 1).

The width of the reservoir B_r does not significantly affect the wave reflection as it can be derived from the similar values of K_r for M2, M3 and M4. The value of B_r can therefore be selected based on the

maximization of the energy production and on the minimization of the costs, while adapting the overall dimension of the device to the spatial constraints posed by the installation in existing breakwaters.

The shape of the sloping plate, instead, affects significantly the reflection phenomenon. The offshore angle of the ramp influences the wave run-up, while the position of the change of the inclination with respect to the sea water level affects the dissipation induced by wave breaking. The configuration M5 shows similar results to M2, except for the first wave condition characterized by the smallest H_{m0}. As a matter of fact, the presence of a vertical element in the ramp shape has a greater influence on the smallest wave height. Therefore, it is important to consider the response of the structure with respect to the wave condition characterized by the greatest frequency in a typical wave climate.

In Figure 9 the values of $q^*_{reservoir}$ for M1–M5 are compared with the results related to M2. The absence of the berm does not change the values of $q^*_{reservoir}$ with respect to M1, at least for the tests characterized by the greatest discharge rates and so the greater wave heights. Therefore, the higher reflection does not change in a significant way the potential power production.

Figure 9. The non-dimensional overtopping flow rate at the rear of the structure, $q^*_{reservoir}$, for the M1–M5 configurations compared with case M2 under normal conditions (Table 1).

The slightly lower values of $q^*_{reservoir}$ for M3 suggest that the reservoir is under-dimensioned. The greater reservoir size of M4 does not lead to a real improvement of the discharge rate. Therefore, it can be concluded that this parameter does not affect significantly the hydraulic performance of the device. Therefore, its design in existing breakwaters has to be focused on the height and the shape of the sloping plate that directly influence the overtopping phenomenon. The dynamic inside the reservoir is more connected to the position of the pipes, which lead the water to flow towards the turbines.

The configuration M5 shows the same result of M2. Therefore, the introduction of a vertical submerged part could be considered to generalize the OBREC cross section, without compromising its hydraulic performance.

3.2. Effects of Geometric Changes on the Structure Loads

The assessment of the loads across the structure has been performed by using numerical pressure transducers, placed in the same position as the experimental ones (Figure 4) to perform a consistent analysis. The results discussed in this section are related to the extreme conditions reported in Table 1. However, the modified geometry required some adaptation for a few cases. The configuration M3

includes 3 sensors along the reservoir due to the reduced value of B_r. In M5 the sensors related to the sloping plate were shifted along the orthogonal direction that links the original inclination to the new ones.

The pressures are analyzed in terms of p_{250}, which corresponds to the non-exceedance level of about 99.7%. Table 4 reports the values related to the sloping plate, the crown wall and the bottom part of the reservoir (uplift pressures).

Table 4. The p$_{250}$ values acting on the sloping plate, the crown wall and the bottom part of the reservoir (uplift pressures) in kPa. See Figure 5 for the gauge locations.

WG No.	Lab	M1	M2	M3	M4	M5
27	1.66	1.68	1.69	1.64	1.77	1.66
28	1.54	1.50	1.53	1.46	1.59	1.47
29	1.44	1.30	1.35	1.26	1.37	1.27
21	1.45	1.09	1.12	1.06	1.15	0.96
26	1.82	1.01	1.07	1.03	1.09	0.79
30	1.96	0.58	0.62	0.76	0.57	0.62
7	2.75	2.18	2.11	2.14	0	2.06
9	2.67	1.77	1.72	1.77	0	1.65
17	2.70	1.52	1.32	1.36	0	1.26
22	1.67	0.97	0.91	0.80	0	0.92
13	2.09	2.30	2.28	2.20	2.30	2.27
12	1.89	2.13	2.11	2.01	2.15	2.10
11	1.84	1.95	1.94	1.81	2.00	1.93
10	1.52	1.75	1.74	/	1.83	1.74

The sample frequency adopted in the numerical model is lower than the laboratory one to minimize the computational effort without compromising the accuracy of the results. A higher sample frequency in the numerical modelling would be required in case the model could reproduce the compressibility of the air, which usually leads to the highest impulsive peaks not so easy to be recorded. Therefore, the numerical results may underestimate the pressures acting on the elements exposed to wave breaking and to the water jet, such as the highest part of the sloping plate and the crown wall.

The configuration M1 reproduces well the experimental values along the sloping plate, with a small underestimation related to the upper part. The configurations M2–M5 show values of p_{250} similar to M1.

The pressures related to the crown wall are very similar for all the configurations. The trend of the physical model is respected, but the discrepancy between the numerical and the experimental results increases from the bottom to the top of the crown wall. Only in the M4 case, all the discharge flows down in the wider reservoir, leading to an unstressed wall even in extreme conditions. This behavior was found to be in agreement with the calculated pressure and physical model measurements on a 1.66 scale of a different overtopping device, named SSG (Seawave Slot-cone Generators) [49]. The authors attributed these differences to the absence of air in the numerical model. Therefore, some pressure peaks reduction (especially in the higher part of the crown wall) when compared to the physical model test could be experienced.

The uplift pressures are well-estimated, leading also to cautious values. This result is very useful considering that the uplift pressures represent the destabilizing force, which play a key role in the overall stability of the breakwaters top element [50].

As anticipated in Section 2.2, the numerical model allows to obtain also the downward pressures where no direct comparison with the experimental data is possible. The statistical values of p$_{250}$ are reported in Table 5. All the configurations show results very similar to each other, being the inshore corner, i.e. corresponding to the gauge 10$_{in}$ (see Figure 4), the most stressed part of the reservoir. This is not completely true for the configurations M4 and M5 due to the size of B_r and to the lower number of overtopping waves, respectively.

Table 5. The pressures acting inside the reservoir in kPa, with the same abscissa of the pressure transducers related to the uplift pressures.

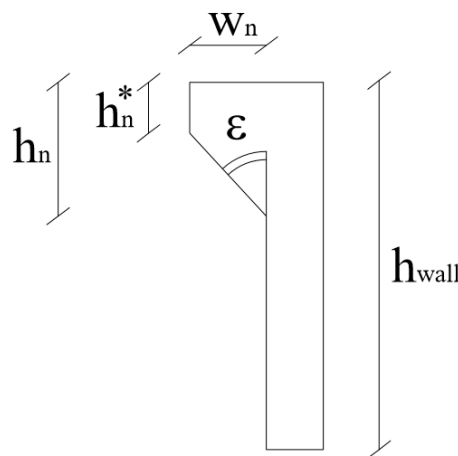| WG No.	Lab	M1	M2	M3	M4	M5
13_{in}	/	1.71	1.73	1.84	1.75	1.77
12_{in}	/	1.60	1.60	1.75	1.54	1.62
11_{in}	/	1.80	1.83	2.06	1.64	1.82
10_{in}	/	2.06	2.07	/	1.83	2.01

3.3. Harbor Safety

The harbor safety has been evaluated in terms of q_{rear}, i.e., the average overtopping discharge at the rear side of the crown wall, in extreme conditions (see Table 1).

For these numerical simulations, the reservoir has been closed to analyze the worst functioning condition, i.e., when the pipe is not capable of draining all the water that overtops the sloping plate.

In the 2012 experimental campaign, for the same wave condition, the values of q_{rear} measured for the OBREC case (Figure 2b) were higher compared to a traditional rubble mound breakwater with similar overall dimensions (Figure 2a) [30]. Therefore, a parapet (nose) has been introduced on the top of the crown wall to increase the safety level of the area inshore the structure. The role of the parapet is to redirect the up-rushing waves back into the front reservoir and towards the sea.

In this study case, the parapet has been designed according to the work performed by Van Doorslaer [51], who investigated the effects of some geometrical parameters on q_{rear}, such as the crown wall height h_{wall}, the extension of the nose h_n and the inclination of the parapet ε (Figure 10).

Figure 10. The scheme of a parapet with all the geometrical parameters.

The larger the angle ε, the higher the wave reflection inside the reservoir is, resulting in smaller values of q_{rear}. The optimal range for ε was found between $30°$ and $45°$, which combines a good reduction of q_{rear} and a limited increase of the pressures on the wall in correspondence to the parapet, i.e., WG22, as shown in Tables 6 and 7. Although the value of ε is the dominant geometric variable, q_{rear} also decreases with increasing h_n (Figure 10). The best reduction was achieved for $\lambda = h_n / h_{wall} \geq 0.3$. Based on these literature results, 2 parapet configurations have been considered, i.e., $\varepsilon = 30°$ and $45°$ and a fixed value of $\lambda = 0.3$. The resulting thickness of the nose w_n is equal to 0.027 m and 0.046 m for $\varepsilon = 30°$ and $45°$, respectively.

Table 6 reports the results of q_{rear} for the OBREC sections with and without the parapet. In the case of the straight crown wall, the greater the reservoir width the lower the overtopping at the rear side of the structure was. The presence of the nose reduces the values of q_{rear} by 34% and by 41%, on average, for $\varepsilon = 30°$ and $45°$, respectively. For both inclinations, the configuration M3 shows the

maximum reduction, i.e., 70% and 80% for $\varepsilon = 30°$ and $\varepsilon = 45°$, respectively. Therefore, the inclusion of the nose leads to a safe harbor area even in case of a constrained reservoir width.

Table 6. The average overtopping discharge at the rear side of the crown wall (q_{rear} (L/s/m)) for cases without parapet and with parapet ($\varepsilon = 30°$ and $45°$ respectively).

	M1	M2	M3	M4	M5
Crown wall	0.47	0.45	0.63	0.00	0.44
Crown wall and parapet ($\varepsilon = 30°$)	0.28	0.30	0.19	0.00	0.31
Crown wall and parapet ($\varepsilon = 45°$)	0.26	0.25	0.13	0.00	0.28

Table 7 shows the values of p_{250} inside the reservoir and along the crown wall to understand the effects, in terms of pressures, of the presence of the nose. Due to the absence of overtopping at the rear side of the structure, the configuration M4 was not analyzed. The results of non-dimensional pressures acting on the crown wall and inside the reservoir are graphically represented in Figures 11 and 12, respectively. In order to provide general results, the relative positions of the pressure transducer have been considered non-dimensionalised. In particular, in Figure 11, the vertical distances from the bottom (z) rather than the wave height (H_{m0}) are shown. In Figure 12, the relative abscissa (x) of pressure transducers from the seaward border of the reservoir has been non-dimensionalised with respect to the reservoir width (B_r).
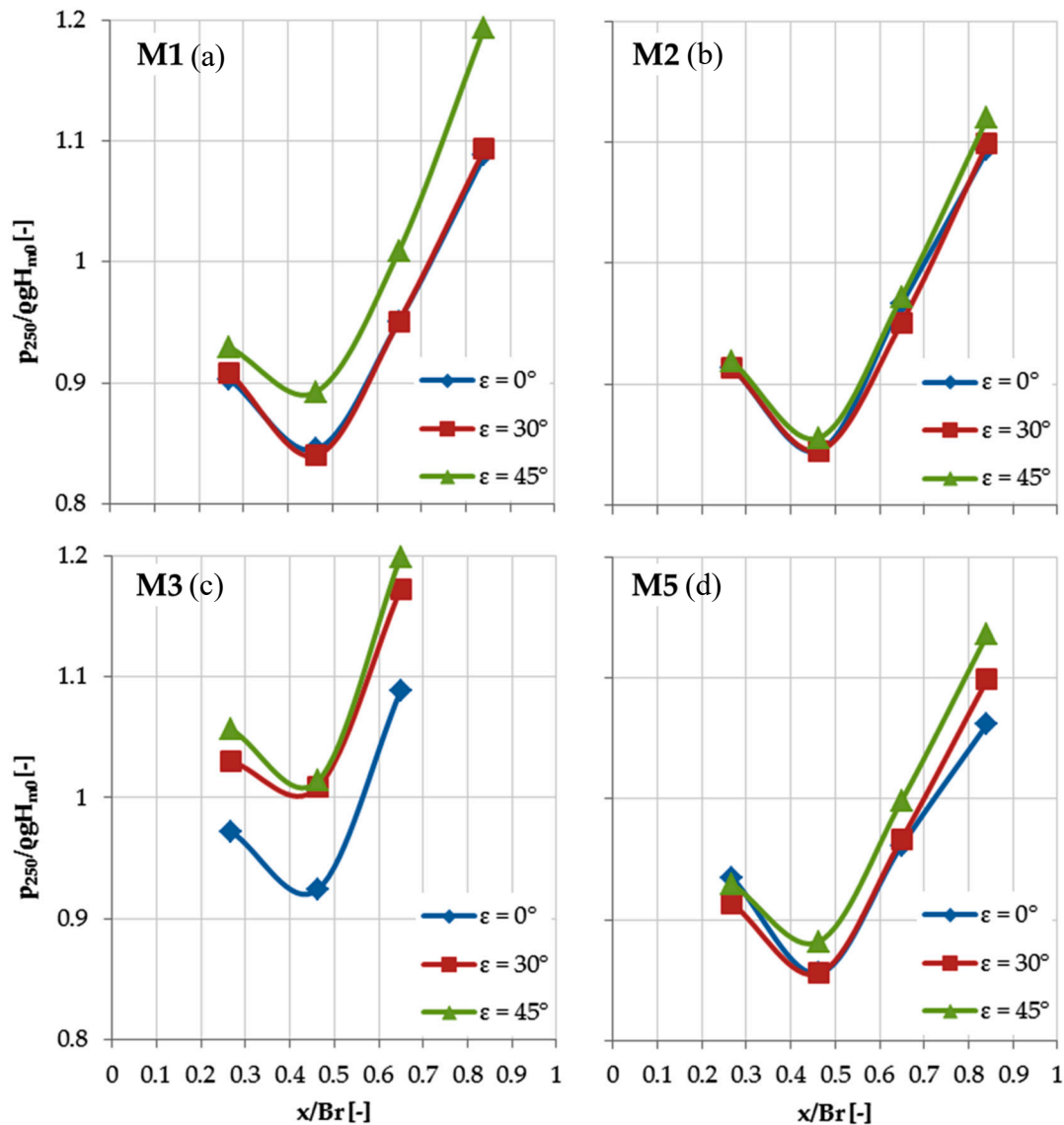
Table 7. Thee p_{250} values inside the reservoir and on the crown wall (kPa), for $\varepsilon = 0°$ (no parapet), $\varepsilon = 30°$ and $\varepsilon = 45°$. The positions of the water gauges (WG) are shown in Figure 4.

Wg	M1	M2	M3	M5
		$\varepsilon = 0°$		
7	2.18	2.11	2.14	2.06
9	1.77	1.72	1.77	1.65
17	1.52	1.32	1.36	1.26
22	0.97	0.91	0.8	0.92
13in	1.71	1.73	1.84	1.77
12in	1.6	1.6	1.75	1.62
11in	1.8	1.83	2.06	1.82
10in	2.06	2.07	/	2.01
		$\varepsilon = 30°$		
7	2.13	2.14	2.32	2.17
9	1.76	1.75	1.93	1.76
17	1.43	1.4	1.56	1.41
22	1.49	1.58	1.28	1.52
13in	1.72	1.73	1.95	1.73
12in	1.59	1.6	1.91	1.62
11in	1.8	1.8	2.22	1.83
10in	2.07	2.08	/	2.08
		$\varepsilon = 45°$		
7	2.39	2.18	2.4	2.23
9	2.05	1.8	2.01	1.85
17	1.88	1.44	1.64	1.57
22	2.38	1.54	1.57	1.83
13in	1.76	1.74	2	1.76
12in	1.69	1.62	1.92	1.67
11in	1.91	1.84	2.27	1.89
10in	2.26	2.12	/	2.15

The presence of the parapet leads to higher pressures on the crown wall, which increase with the increasing of ε. The downward pressures are almost constant for all the configurations due to the

load dampening caused by the presence of the water inside the reservoir, which is always saturated. Only for M3, the computed statistical values are slightly higher due to the reduced value of B_r.

Therefore, the OBREC design has to consider the introduction of a parapet to reduce the overtopping at the rear side of the structure. The best configuration which optimizes the values of q_{rear} implied the parapet be inclined at 45° without increasing the pressures. The other geometric parameters, i.e., the berm and the reservoir width, do not affect q_{rear} and p_{250}.

Figure 11. The non-dimensional pressures on the crown wall for the configurations (**a**) M1, (**b**) M2, (**c**) M3 and (**d**) M5. The vertical distances from the bottom (z) rather than the wave height (H_{m0}) are reported on the ordinate, while the statistical values of p_{250} divided by the wave height (H_{m0}), the density (ρ) and the gravitational acceleration (g), on the abscissa.

Figure 12. The non-dimensional pressures inside the reservoir for the configurations (**a**) M1, (**b**) M2, (**c**) M3 and (**d**) M5. The statistical values of p_{250} divided by the wave height (H_{m0}), the water density (ρ) and the gravitational acceleration (g) are reported on the ordinate; while the relative abscissa (x) of pressure transducers from the seaward border of the reservoir has been non-dimensionalised with respect to the reservoir width (Br), on the abscissa.

4. Discussion of the Results with Reference to the Prototype Installation

The test campaigns performed during 2012 and 2014 were aimed to understand the general behavior of the OBREC device and the relevance of its elements on the hydraulic and structural performances. However, to establish the fraction of extractable resource and safety performance, more detailed considerations were required. In principle, there is not "the best" OBREC cross section that may be used everywhere. It is expected that, depending on the selected site characteristics, some shape of the sloping plate could be more efficiently used than others. In any case, the selection of the optimal OBREC configuration is a complex matter which cannot be done in a brief overview. For a site-specific installation, in fact, the design considerations have to be tuned based on the operating (normal) and extreme wave climate at the site. The design has to also account for the spatial constraints due to the harbor layout and the configuration of the existing breakwaters.
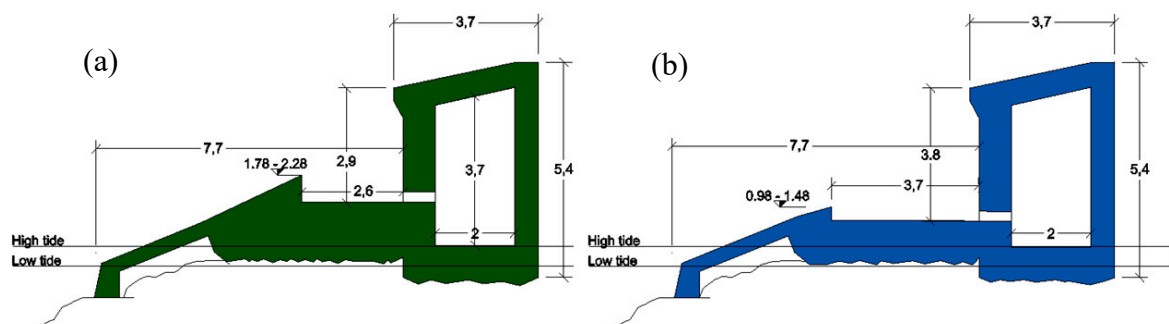
The main result observed from the numerical simulations here reported that the enhancement of $q^*_{reservoir}$ could increase the values of q_{rear}. In particular, assuming that the water jets follow the tangent of the ramp crest, which works as a deflector, the greater the hydraulic performances of the frontal sloping ramp, the greater the value of up-rushing water driven directly on the upper part of the crown wall is. This means a potential higher overtopping discharge at the rear of the structure and a higher pressure on the parapet.

Looking to the tested configurations, one of the best compromises is represented by the double shaped sloping plate (configuration M5). This kind of cross section does not affect significantly the wave overtopping inside the reservoir and is able to reduce the overtopping at the rear of the structure and also if a crown wall without a nose is considered. Then, not so high values of wave loading are measured. Furthermore, the idea behind M5 is to define a more general cross section, which can be easily placed on top of existing breakwaters independently from its off-shore slope. Therefore, the double plates configuration was considered for the first OBREC pilot plant (Figure 13). The prototype was installed in the San Vincenzo breakwater, located in the port of Naples [52].

Figure 13. The OBREC prototype installed in the San Vincenzo breakwater, port of Naples.

The prototype cross section includes two configurations, i.e., NW-LAB (Natural Waves LABoratory) and RS-LAB (Real Scale LABoratory) shown in Figure 14.

Figure 14. The cross sections of the OBREC prototype installed in the Naples harbor: (**a**) the RS-LAB (Real Scale Laboratory) configuration and (**b**) the NW-LAB (Natural Waves Laboratory) configuration.

They are characterized by the same longitudinal dimension, having in common the rear wall and the room for the turbines (Figure 14). This leads to the main geometric differences in the frontal part of the device. Indeed, they differ mainly in the height of the sloping plate R_r, and to meet the same spatial constraints, they have different dimensions of the reservoir width B_r. The two values of R_r have been selected according to the analysis of the typical wave climate of the site and to take into account the different turbine technologies, working with a different nominal head. The intention is not only to provide results for the sea climate at the study site but also to gather useful data easily exportable for more energetic sites. According to the analysis of the typical wave climate, the selected values of R_r for NW-LAB and RS-LAB are 1.2 m and 2.0 m respectively (values referred to the mean tide level). The corresponding values of the reservoir width are 2.6 m and 3.7 m. The lower value of R_r was selected according to the mean run-up of the most frequent wave (i.e., $H_s = 0.8$ m). The upper value of R_r was intended to capture the higher power generated by the higher waves. Its definition, however, followed a different approach. If one look at the maximum value of the power was multiplied by the wave frequency of occurrence (F), the prevalent wave height is associated to $H_{m0} = 2.2$ m, $T_p = 6.8$ s. In this case, however, the yearly average frequency of occurrence is too low ($F = 1.4\%$) corresponding to just five days per year. Therefore, considering that the lowest nominal hydraulic head of the greatest low head Kaplan turbine [53] is 1.5 m, a ramp crest of about 2 m ($1.78 \div 2.28$ m for low- and high-water levels respectively) has been selected. This value can guarantee an average of about 30 equivalent working days per year of the RS-LAB (the name Real Scale, hence, indicates the site-specific considerations made for that ramp crest).

Figure 14 shows, separately, the actual 2D OBREC cross sections, resulting from some modifications on the original project presented in Contestabile [33]. It is possible to recognize some geometrical details derived from the results obtained from the experiments and the numerical simulations here presented. For instance, the submerged quasi-vertical part of the ramp has been introduced to improve the ramp resistance to bending and to fatigue. Furthermore, the interlocking between the rocks of the armour layer and the device is also enhanced.

As shown in Figure 12, the smaller reservoir is associated to the higher sloping plate and vice versa. In the first case, the number of overtopped waves is lower and can be handled by a reduced dimension of B_r. The wider reservoir is more appropriate for the lower sloping plate, which is overtopped more frequently. The sensitivity of this parameter with respect to the hydraulic and structural performance, as it has been demonstrated during the experimental and numerical analysis, can be neglected. Therefore, the selection of B_r can be done after the design of R_r.

To guarantee the harbor safety at the inshore area of the structure, a parapet has been placed on the crown wall. The effectiveness of this element increases as the dimension of the reservoir width decreases, ensuring an adequate safety level for both the configurations.

Differently from the laboratory and the numerical models, the prototype cross sections (Figure 14) are provided with a wave chamber where a new set of turbines is going to be installed to produce electricity. The bottom elevation of the chamber maximizes its difference with respect to the sea water level. The chamber is linked with the reservoirs by means of holes (Figure 14) and five pipes (Figure 14). The lowest hole along the wall aims to collect as much water as possible, maximizing the energy exploitation. The position and the size of the holes and the pipes have not been yet investigated due to the limitations of testing in 2-D conditions. For this reason, a 3-D investigation, capable of reproducing the dynamics between the reservoir and the wave chamber, is needed. The 3-D numerical modelling of the OBREC pilot plant, which is composed by the two configurations here analysed, could improve the representation of the discharge rates. The realistic representation of the pipes can be the key to defining the design criteria to maximize the energy production.

5. Conclusions

The general aim of this paper was to assess the relevance of some geometrical elements of the OBREC cross section in the hydraulic and structural performances. For this purpose, a 2-D numerical model of the OBREC device was calibrated in order

- to extend the experimental database of the laboratory tests performed in 2012 and in 2014 and
- to perform a sensitivity analysis related to the elements composing its cross section.

The elements examined during the sensitivity analysis were
(a) the presence of the berm;
(b) the shape of the sloping plate and the introduction of a parapet on the rear wall; and
(c) the reservoir width.

The inclusion of the berm does not change significantly the $q_{reservoir}$ or the pressure distribution along the structure. However, it slightly increases K_r as expected, suggesting the design of a toe protection.

The investigation of a double inclination in the ramp shape was aimed to generalize the OBREC cross section. However, the analysis performed showed that the position of the inclination change is more sensitive than the values of the slope angles. Therefore, it is suggested to locate the slope change point under the still water level in order to minimize the energy losses due to the wave breaking. The benefits of the double-shaped frontal ramp are emphasized considering the effective sloping ramp configuration of the OBREC full scale prototype. In fact, for the OBREC installation above an existing breakwater, the use of prefabricated structures is strongly recommended. In such conditions, a single slope plate is quite difficult to build due to construction requirements. Therefore, the prefabricated ramps cross section can be conveniently constituted by two elements:

1. an auxiliary submerged part with a subvertical face (aimed to improve the ramp resistance to bending and to fatigue) and

2. an emerged plate with the slope angle designed to improve the overtopping of a specific range of wave amplitude and wave frequency.

The reservoir width does not significantly affect the values of K_r and p_{250}, except for the wider reservoir that leads to an unstressed rear wall. Therefore, B_r can be selected after the design of the sloping plate, which appeared to be the most sensitive element.

To ensure the harbor safety of the inshore area of the structure, 2 parapets configurations have been analyzed. In extreme conditions, the parapet inclined of 30° reduces the values of q_{rear} by 34%, while the one inclined at 45° was reduced by 41%, on average. The maximum reduction has been measured for the configuration characterized by the smallest reservoir width, i.e., 70% and 80% for $\varepsilon = 30°$ and $\varepsilon = 45°$, respectively. Therefore, the inclusion of the inclined parapet leads to a safer harbor area even in case of constrained values of B_r. The best results have been obtained for the parapet inclined of 45°, which optimizes the values of q_{rear} without increasing the pressures.

References

1. Brooke, J. (Ed.) *Wave Energy Conversion*; Elsevier: Oxford, UK, 2003.
2. Clement, A.; McCullen, P.; Falcao, A.; Fiorentino, A.; Gardner, F.; Hammarlund, K.; Lemonis, G.; Lewis, T.; Nielsen, K.; Petroncini, S.; et al. Wave energy in Europe: Current status and perspectives. *Renew. Sustain. Energy Rev.* **2002**, *6*, 405–431. [CrossRef]
3. Falnes, J. (Ed.) *Ocean Wave Energy*; Cambridge University Press: Cambridge, UK, 2002.
4. BLUENE Project. Available online: http://www.medmaritimeprojects.eu/section/bluene (accessed on 30 January 2019).
5. EnviCOP Project—EnviCOP. Available online: http://cordis.europa.eu/project/rcn/102427_en.html (accessed on 30 January 2019).
6. Contestabile, P.; Vicinanza, D. Coastal Defence Integrating Wave-Energy-Based Desalination: A Case Study in Madagascar. *J. Mar. Sci. Eng.* **2018**, *6*, 64. [CrossRef]
7. Rodriguez-Delgado, C.; Bergillos, R.J.; Ortega-Sánchez, M.; Iglesias, G. Protection of gravel-dominated coasts through wave farms: Layout and shoreline evolution. *Sci. Total Environ.* **2018**, *636*, 1541–1552. [CrossRef] [PubMed]
8. Rodriguez-Delgado, C.; Bergillos, R.J.; Ortega-Sánchez, M.; Iglesias, G. Wave farm effects on the coast: The alongshore position. *Sci. Total Environ.* **2018**, *640*, 1176–1186. [CrossRef] [PubMed]
9. Rodriguez-Delgado, C.; Bergillos, R.J.; Iglesias, G. Dual wave farms and coastline dynamics: The role of inter-device spacing. *Sci. Total Environ.* **2019**, *646*, 1241–1252. [CrossRef] [PubMed]
10. Bergillos, R.J.; Rodriguez-Delgado, C.; Iglesias, G. Wave farm impacts on coastal flooding under sea-level rise: A case study in southern Spain. *Sci. Total Environ.* **2019**, *653*, 1522–1531. [CrossRef] [PubMed]
11. Pelc, R.; Fujita, R.M. Renewable energy from the ocean. *Marine Policy* **2002**, *26*, 471–479. [CrossRef]
12. Villate, J. Situacion actual dela senergías marinas y perspectivas de futuro. In Proceedings of the Seminario Annual de Automatica, Electronica e Instrumentacion (SAAEI), Bilbao, Spain, 8 October 2010.
13. Chozas, J.F.; Sørensen, H.C.; Jensen, N.H. Economic benefit of combining wave and wind power productions in day-ahead electricity markets. In Proceedings of the 4th International Conference on Ocean Energy, Dublin, Ireland, 17–19 October 2012.
14. Astariz, S.; Iglesias, G. The economics of wave energy: A review. *Renew. Sustain. Energy Rev.* **2015**, *45*, 397–408. [CrossRef]
15. Falcão, A.D.O.; Pereira, P.E.R.; Henriques, J.C.C.; Gato, L.M.C. Hydrodynamic simulation of a floating wave energy converter by a U-tube rig for power take-off testing. *Ocean Eng.* **2010**, *37*, 1253–1260. [CrossRef]
16. TROPOS Project. Available online: http://www.troposplatform.eu (accessed on 13 December 2018).
17. MERMAID Project. Available online: http://www.mermaidproject.eu (accessed on 13 December 2018).
18. H2OCEAN Project. Available online: http://www.h2ocean-project.eu (accessed on 13 December 2018).
19. Zanuttigh, B.; Angelelli, E.; Bellotti, G.; Krontira, Y.; Suffredini, R.; Airoldi, L.; Franceschi, G.; Troianos, D.; Romano, A.; Zagonari, F.; et al. Boosting blue growth in a mild Sea: Analysis of the synergies produced by a multi-purpose offshore installation in the Northern Adriatic, Italy. *Sustainability* **2015**, *7*, 6804–6853. [CrossRef]
20. Zanuttigh, B.; Angelelli, E.; Kortenhaus, A.; Koca, K.; Krontira, Y.; Koundouri, P. Methodology for multi-criteria design of multi-use offshore platforms for marine renewable energy harvesting. *Renew. Energy* **2016**, *85*, 1271–1289. [CrossRef]
21. Contestabile, P.; Lauro, E.D.; Galli, P.; Corselli, C.; Vicinanza, D. Offshore wind and wave energy assessment around Malè and Magoodhoo Island (Maldives). *Sustainability* **2017**, *9*, 613. [CrossRef]
22. Azzellino, A.; Lanfredi, C.; Contestabile, P.; Ferrante, V.; Vicinanza, D. Strategic environmental assessment to evaluate WEC projects in the perspective of the environmental cost-benefit analysis. In Proceedings of the Twenty-First International Offshore and Polar Engineering Conference, Maui, HI, USA, 19–24 June 2011.
23. Perez-Collazo, C.; Greaves, D.; Iglesias, G. A review of combined wave and offshore wind energy. *Renew. Sustain. Energy Rev.* **2015**, *42*, 141–153. [CrossRef]
24. Boccotti, P. Caisson breakwaters embodying an OWC with a small opening–Part I: Theory. *Ocean Eng.* **2007**, *34*, 806–819. [CrossRef]

25. Pecher, A.; Kofoed, J.P.; Le Crom, I.; Neumann, F.; Azevedo, E.D.B. Performance assessment of the Pico OWC power plant following the EquiMar Methodology. In Proceedings of the Twenty-First International Offshore and Polar Engineering Conference, Maui, HI, USA, 19–24 June 2011.

26. Boake, C.B.; Whittaker, T.J.; Folley, M.; Ellen, H. Overview and initial operational experience of the LIMPET wave energy plant. In Proceedings of the Twelfth International Offshore and Polar Engineering Conference, Kitakyushu, Japan, 26–31 May 2002.

27. Torre-Enciso, Y.; Ortubia, I.; López de Aguileta, L.I.; Marqués, J. Mutriku wave power plant: From the thinking out to the reality. In Proceedings of the 8th European Wave Tidal Energy Conference, Uppsala, Sweden, 7–10 September 2009; pp. 319–329.

28. Marqués, J.; López de Aguileta, L.I.; Torre-Enciso, Y. Mutriku. Lessons learnt. In Proceedings of the 3rd International Conference on Ocean Energy, Bilbao, Spain, 6–8 October 2010.

29. Vicinanza, D.; Frigaard, P. Wave pressure acting on a seawave slot-cone generator. *Coast. Eng.* **2008**, *55*, 553–568. [CrossRef]

30. Vicinanza, D.; Contestabile, P.; Harck Nørgaard, J.; Lykke Andersen, T. Innovative rubble mound breakwaters for overtopping wave energy conversion. *Coast. Eng.* **2014**, *88*, 154–170. [CrossRef]

31. Iuppa, C.; Contestabile, P.; Cavallaro, L.; Foti, E.; Vicinanza, D. Hydraulic performance of an innovative breakwater for overtopping wave energy conversion. *Sustainability* **2016**, *8*, 1226. [CrossRef]

32. Contestabile, P.; Iuppa, C.; Di Lauro, E.; Cavallaro, L.; Andersen, T.L.; Vicinanza, D. Wave loadings acting on innovative rubble mound breakwater for overtopping wave energy conversion. *Coast. Eng.* **2017**, *122*, 60–74. [CrossRef]

33. Contestabile, P.; Ferrante, V.; Di Lauro, E.; Vicinanza, D. Prototype Overtopping Breakwater for Wave Energy Conversion at Port of Naples. In Proceedings of the 26th International Conference ISOPE, Rhodes, Greece, 26 June–1 July 2016; pp. 616–621.

34. Losada, I.J.; Lara, J.L.; Guanche, R.; Gonzales-Ordina, J.M. Numerical analysis of wave overtopping of rubble mound breakwaters. *Coast. Eng.* **2008**, *55*, 47–62. [CrossRef]

35. Forchheimer, P. Wasserbewegung durch Boden. *Z. Ver. Deutsch. Ing.* **1901**, *45*, 1782–1788.

36. Van Gent, M.R.A. Porous flow through rubble-mound material. *J. Waterw. Port Coast. Ocean Eng.* **1995**, *121*, 176–181. [CrossRef]

37. Lynett, P.J.; Liu, P.L.-F.; Losada, I.J. Vidal, C. Solitary Wave Interaction with Porous Breakwater. *J. Waterw. Port Coast. Ocean Eng.* **2000**, *126*, 314–322. [CrossRef]

38. Hsu, T.J.; Sakakiyama, T.; Liu, P.L.F. A numerical model for wave motions and turbulence flows in front of a composite breakwater. *Coast. Eng.* **2002**, *46*, 25–50. [CrossRef]

39. Romano, A.; Bellotti, G.; Briganti, R.; Franco, L. Uncertainties in the physical modelling of the wave overtop-ping over a rubble mound breakwater: The role of the seeding number and of the test duration. *Coast. Eng.* **2014**, *103*, 15–21. [CrossRef]

40. Mansard, E.P.; Funke, E.R. The measurement of incident and reflected spectra using a least squares method. In *Coastal Engineering 1980*; American Society of Civil Engineers: Reston, VA, USA, 1980; pp. 154–172.

41. Palma, G.; Contestabile, P.; Mizar Formentin, S.; Vicinanza, D.; Zanuttigh, B. Design optimization of a multifunctional wave energy device. In *Progress in Renewable Energies Offshore, Proceedings of the 2nd International Conference on Renewable Energies Offshore (RENEW2016), Lisbon, Portugal, 24–26 October 2016*; CRC Press: Boca Raton, FL, USA, 2016; p. 235.

42. Ahrens, J.P.; Heimbaugh, M.S. Irregular wave overtopping of seawalls. In Proceedings of the OCEANS'86, Washington, DC, USA, 23–25 September 1986; pp. 96–103.

43. EurOtop 2016. Available online: http://www.overtopping-manual.com/ (accessed on 13 December 2018).

44. Willmott, C.J. On the validation of models. *Phys. Geogr.* **1981**, *2*, 184–194. [CrossRef]

45. Kofoed, J.P. Wave Overtopping of Marine Structures—Utilization of Wave Energy. Ph.D. Thesis, Hydraulics Coastal Engineering Laboratory, Department of Civil Engineering, Aalborg University, Aalborg, Denmark, December 2002.

46. Nam, B.W.; Shin, S.H.; Hong, K.Y.; Hong, S.W. Numerical simulation of wave flow over the spiral-reef overtopping device. In Proceedings of the Eighth ISOPE Pacific/Asia Offshore Mechanics Symposium, Jeju, Korea, 14–17 October 2008.

47. Zanuttigh, B.; Van Der Meer, J.W.; Andersen, T.L.; Lara, J.L.; Losada, I.J. Analysis of wave reflection from structures with berms through an extensive database and 2DV numerical modelling. In Proceedings of the Coastal Engineering 2008, Hamburg, Germany, 31 August–5 September 2008; Volume 5, pp. 3285–3297.

48. Formentin, S.M.; Palma, G.; Contestabile, P.; Vicinanza, D.; Zanuttigh, B. DV RANS-VOF numerical modeling of a multi-functional harbor structure. *Coast. Eng. Proc.* **2017**, *1*, 3. [CrossRef]

49. Buccino, M.; Dentale, F.; Salerno, D.; Contestabile, P.; Calabrese, M. The use of CFD in the analysis of wave loadings acting on seawave slot-cone generators. *Sustainability* **2016**, *8*, 1255. [CrossRef]

50. Goda, Y. A new method of wave pressure calculation for the design of composite breakwater. *Rep. Port Harb. Res. Inst.* **1973**, *12*, 31–70. (In Japanese)

51. Van Doorslaer, K.; De Rouck, J.; Audenaert SDuquet, V. Crest modifications to reduce wave overtopping of non-breaking waves over a smooth dike slope. *Coast. Eng.* **2015**, *101*, 69–88. [CrossRef]

52. Contestabile, P.; Ferrante, V.; Di Lauro, E.; Vicinanza, D. Full-scale prototype of an overtopping breakwater for wave energy conversion. *Coast. Eng. Proc.* **2017**, *1*, 12. [CrossRef]

53. VLH Turbine. Available online: http://www.vlh-turbine.com/products/vlh-turbine/ (accessed on 13 December 2018).